Green Energy and Resources 4 (2026) 100189

Contents lists available at ScienceDirect

Green Energy and Resources

journal homepage: www.journals.elsevier.com/green-energy-and-resources

Research Article

Development of similarity and normalization models for spray characteristics with the momentum equation as the theoretical basis

Meiqi Yu[a], Hongliang Luo[b], Weidi Huang[b], Pengbo Dong[c], Yu Jin[d], Keiya Nishida[e], Chang Zhai[b,*], Xiaoqing Tian[f]

[a] College of Mechanical and Electrical Engineering, Harbin Engineering University, Harbin, 150001, China
[b] College of Power and Energy Engineering, Harbin Engineering University, Harbin, 150001, China
[c] Institute of Internal Combustion Engines, Dalian University of Technology, Dalian, 116024, China
[d] Institute for Energy Research, Jiangsu University, Zhenjiang, 212013, China
[e] Department of Mechanical System Engineering, University of Hiroshima, 1-4-1 Kagamiyama, Higashi-Hiroshima, 739-8527, Japan
[f] International School, Binzhou Polytechnic, Binzhou, 256603, China

ARTICLE INFO

Keywords:
0.07 mm hole diameter
300 MPa injection pressure
Normalized mathematical model

ABSTRACT

Fuel atomization in diesel engines can be significantly improved by elevating the injection pressure and decreasing the nozzle orifice diameter. Addressing the limited research on mathematical modeling within the regime of 300-MPa-level injection and micro-holes, this paper presents a comprehensive study on the similarity and normalization of spray evolution for ultra-high-pressure micro-nozzle configurations. In the experiments, key parameters such as injection pressure difference, ambient density, and hole diameter were selected as the main variables. The spray development process was divided into two main stages, and the similarity criteria and normalization equations for spray characteristics were derived accordingly. Combined with the DBI (Diffused Back-Illumination) method and processing technology, experimental data were obtained to verify the reliability of the established models. The experimental results show that both the similarity conversion results and normalization results of the derived mathematical models exhibit good consistency with the experimental data. This study can provide theoretical support for the optimization and spray characteristic prediction of ultra-high pressure small high-speed diesel engines.

1. Introduction

Owing to its core advantages including high thermal efficiency, high torque output, excellent mechanical reliability, and superior operating condition adaptability, the diesel engine has become the primary power source for core equipment in key national economic and defense fields such as agricultural machinery, national defense and military equipment, marine power systems, engineering machinery, and heavy-duty commercial vehicles (Ouyang et al., 2019; Xin, 2011; Gerald Liu and Munnannur, 2019; Murugesan et al., 2009). With regard to the operating mechanism of diesel engines, the fuel atomization process and in-cylinder combustion characteristics are the core key parameters that determine the overall performance of the engine. The formation and homogeneity of the in-cylinder air-fuel mixture are fundamentally dictated by the effectiveness of fuel atomization, while the uniformity of the fuel-air mixture further dominates the sufficiency of the combustion reaction. This cascading process directly affects the thermal efficiency, power density, dynamic response characteristics, and emission characteristics of the diesel engine (Pandey et al., 2012; Zhou et al., 2024; Park et al., 2013; Xia et al., 2019; Zhang et al., 2026). In brief, achieving superior fuel atomization quality and more efficient homogeneous combustion constitutes the core breakthrough for diesel engines to realize energy conservation, consumption reduction, power enhancement, efficiency improvement, and emission and pollution reduction. A large number of relevant research findings have fully confirmed that reducing the hole diameter of injectors and increasing the fuel injection pressure are effective technical approaches to improve the fuel atomization performance (Mohan et al., 2013; Chen et al., 2013; Zhai et al., 2021a,b; Zhai et al., 2021, 2021; Kothiwale et al., 2023). A smaller hole diameter enables the fuel jet to form a finer initial fuel spray at the moment of injection, significantly enhancing the primary breakup effect of the fuel jet; higher injection pressure can endow the fuel jet with

* Corresponding author.
E-mail address: changzhai@hrbeu.edu.cn (C. Zhai).

https://doi.org/10.1016/j.gerr.2026.100189
Received 23 January 2026; Received in revised form 10 May 2026; Accepted 14 May 2026
2949-7205/© 2026 The Authors. Published by Elsevier B.V. on behalf of Shandong University. This is an open access article under the CC BY license (http://creativecommons.org/licenses/by/4.0/).

stronger initial kinetic energy, intensify the impact, shear, and entrainment effects between the fuel jet and the in-cylinder air, and accelerate the secondary breakup, evaporation, and mixing processes of the fuel spray. Driven by the imperative for environmental sustainability and superior thermal efficiency, the escalation of fuel injection pressures has solidified as a fundamental trajectory in modern diesel engine innovation. Consequently, ultra-high-pressure injection systems have emerged as a pivotal research frontier for the development of next-generation clean powerplants. Nevertheless, transitioning into the ultra-high-pressure regime potentially triggers a fundamental shift in fuel jet disintegration mechanisms and spray morphology. Existing empirical correlations derived from conventional pressure ranges often fail to capture these complex dynamics, rendering them inadequate for modern ultra-high-pressure applications (Zhai et al., 2021a,b; Zhai et al., 2021a,b; Yu et al., 2026). Consequently, a systematic exploration of spray evolution at these extreme scales is not only scientifically imperative for advancing atomization theory but also strategically essential for the technological progression of high-performance diesel engines.

Extensive literature has documented the spray and combustion phenomena associated with micro-orifices and intensified injection pressures. Digital imaging was utilized by Delacourt et al. (2005) to analyze diesel sprays at 80–250 MPa, while Wang et al. (2019) leveraged piezoelectric injectors to study similar pressure ranges. At even higher intensities, the spray-induced shock waves and mixing efficiencies were investigated by Jia et al., 2016a,b; 2016) and Vera-Tudela et al. (2020), with the latter exploring pressures reaching 500 MPa. Furthermore, the present authors have previously conducted comprehensive assessments of how nozzle hole number, fuel properties, and ambient parameters influence atomization under these ultra-high-pressure micro-hole constraints (Zhai et al., 2021a,b; Zhai et al., 2021a,b; Zhai et al., 2022a,b; Luo et al., 2023; Zhai et al., 2023a,b; Zhai et al., 2022a,b; Zhai et al., 2023a,b; Zhai et al., 2025). The results demonstrate that the fuel spray under ultra-high pressure may undergo expansion and other phenomena in the downstream region and exhibits stronger entrainment and a lower equivalence ratio. In addition, the combination of ultra-high pressure and micro-holes results in reduced soot formation.

The spray low-dimensional prediction model is one of the most classical and core simplified models applied in the numerical modeling of internal combustion engines, featuring advantages such as high computational efficiency, extremely low computing power demand, ultra-fast operation speed, simple model structure, and clear physical concepts. Prominent among these predictive frameworks are the phenomenological penetration model introduced by Hiroyasu and the widely utilized penetration correlation developed by Naber and Siebers. (Hiroyasu and Arai, 1990; Siebers, 1998; Wakuri C et al., 1960; Dent, 1971; Arrègle et al., 1999). With the advancement of technology, numerous scholars have also carried out research on low-dimensional spray models. To enhance prediction accuracy during the early spray stages, a penetration model incorporating the sac pressurization dynamics at the start of injection (SOI) was advanced by Zhou and Li (2021). Furthermore, the temporal evolution of spray tip penetration relative to the time elapsed since injection has been effectively characterized by Kostas et al. (2009) using an exponential fitting function in the form of $S_{(t)} = At^{1.5}$.

To enhance the predictive fidelity of spray tip penetration, momentum-based modeling approaches were integrated by researchers such as Desantes and Payri (Desantes et al., 2006a,b; Desantes et al., 2006a,b). More recently, the exploration of spray dynamics has been extended to extreme regimes; for instance, An et al. (2025) performed a comprehensive experimental and theoretical assessment of spray evolution characterized by large-scale orifices and high background densities, reaching injection pressures as high as 270 MPa. During the research on spray models and characteristics, it has been found that both spray morphology and combustion behavior possess inherent similarities when evaluated across a diverse range of operational parameters (Jin et al., 2020; Stager and Reitz, 2007; Shi and Reitz, 2008; Zhou et al., 2018). The utilization of such similarities can substantially reduce the cost of engine design and optimization, while enhancing the accurate predictability of the models. Scaling methodologies for critical engine parameters were explored by Bergin and Stager et al. (Stager and Reitz, 2007; Bergin et al., 2005), who integrated the Hiroyasu & Arai model with Pickett's flame lift-off correlations to analyze spray and combustion development. Regarding the mathematical representation of spray evolution, Suzuki et al. (Suzuki and Ohshima, 2002) derived dimensionless expressions for tip penetration based on breakup time and length under varying injection intensities. This dimensionless approach was further synthesized by Arai (Arai, 2022) to establish a normalized penetration framework. Furthermore, the principles of geometric similarity were extended by Inagaki et al. (2016) to investigate spray behavior across different cylinder scales, resulting in a novel theoretical framework for spray similarity.

In summary, although a preliminary framework for ultra-high pressure micro-hole injection has been proposed, a unified theoretical description of the similarity and normalization issues remains lacking. In this study, we established a rigorous time-scale-based normalization theory by extending the spatiotemporal scaling framework we previously proposed (Zhai et al., 2024). A set of closed-form normalization equations was derived accordingly, which can clearly describe the jet evolution process under extreme injection intensities. The results show that the proposed formulas successfully collapse the spray characteristics obtained under different injection conditions into a unified similarity space, revealing the dominant role of time-scale normalization in controlling the spray evolution process. These findings provide, for the first time, a unified theoretical basis for the normalization of ultra-high pressure jets and offer a practical modeling framework for engine design and optimization.

2. Experimental conditions and setup

The physical configurations and technical specifications of the nozzles are detailed in Fig. 1 and Table 1. For this investigation, solenoid-actuated diesel injectors (manufactured by Denso) equipped with mini-sac nozzles were selected. The measurement campaign incorporated two distinct injectors, differing in their orifice diameters (0.07 and 0.101 mm) but sharing a constant included angle of 155°. Furthermore, the orifice length and sac cavity radius were uniformly maintained at 0.8 and 0.5 mm, respectively, across both hardware configurations.

The specific testing environment and physical properties of the fuel are summarized in Table 2 and Table 3. Standard JIS #2 diesel, possessing a nominal density of 830 kg/m^3, served as the primary test fluid. Throughout all test cases, the energizing duration was strictly fixed at 2.3 ms. To explore the characteristics of ultra-high-pressure injection, the common rail pressure was systematically regulated across a range from 100 to 300 MPa. Inert nitrogen gas was supplied to the constant-volume chamber to establish three distinct ambient density conditions: 10, 15, and 20 kg/m^3. Under a well-controlled ambient temperature of 300 K, these specific density settings yielded corresponding absolute background pressures of 0.88, 1.32, and 1.76 MPa, respectively.

To quantify spray morphology, a Diffused Back-Illumination (DBI) technique was implemented, with the complete optical configuration depicted in Fig. 2. The diagnostic setup utilized an LED cold light source coupled with a diffuser plate to generate a uniform field of scattered light. This light passed through the constant volume combustion vessel, where it was attenuated by the evolving fuel spray before being recorded by a high-speed imaging system. The acquisition was performed using a NAC MEMRECAM HX-3 camera equipped with a Nikon 105 mm (f/4.8) lens. The camera was configured with a frame rate of 40000 fps at a resolution of 640 × 640 pixels, with an exposure time of 50 μs. Diverging from simplified single-hole studies, this work employed a production-standard 10-hole injector. The injector was mounted at a 37.5°

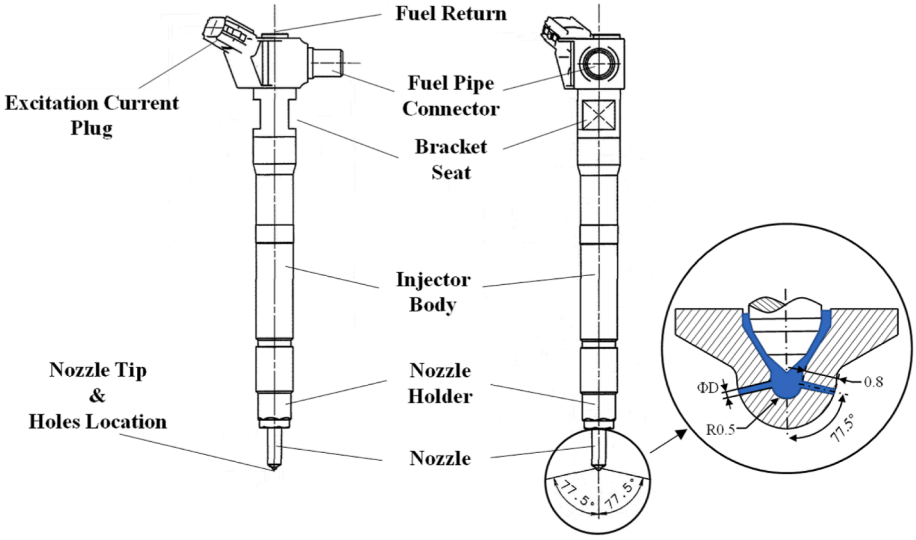


Fig. 1. Internal structure of nozzle.

Table 1
Technical characteristics of the injectors utilized in this work.

Items	Value
Manufacturer company	Denso
Type	Mini-Sac
Hole numbers	10
Outlet umbrella angle [°]	155
Orifice diameter [mm]	0.07/0.101
Length of hole [mm]	0.8
Sac radius [mm]	0.5

Table 2
Detailed operating parameters and ambient environments for spray testing.

Parameter	Value
Fuel specification	Diesel (JIS#2)
Injection duration [ms]	2.3
Injection pressure [MPa]	100-300
Back gas of chamber	Nitrogen
Back density [kg/m^3]	10; 15; 20
Back temperature[K]	300
Back pressure [MPa]	0.88; 1.32; 1.76

Table 3
Detailed characteristics of the JIS#2 diesel fuel.

Property	Value
JIS#2l Density @ 15 °C [kg/m^3]	≈ 830
JIS#2 Kin.Viscosity @ 30 °C [mm^2/s]	>2.5
JIS#2 Flash Point [°C]	>60
JIS#2 Sulfur Content [ppm]	<10

inclination to the horizontal plane. As highlighted in Fig. 2, the target spray (visualized in red) maintained a 25° trajectory relative to the vertical axis, necessitating a geometric correction factor of 1/cos25° during subsequent data analysis to retrieve actual penetration distances.

Fig. 3 illustrates the processing procedure of the spray images. Specifically, the background image (A_1) was subtracted from the spray image (A_2), followed by binarization processing with a threshold value of 10%, yielding the binarized image (A_3) as shown in Fig. 3. The central region of this image corresponds to the target spray. The spray tip penetration (S) is characterized as the maximum longitudinal displacement from the nozzle orifice to the advancing edge of the fuel plume. Simultaneously, the spray angle (θ) is determined by measuring the angular width of the spray boundaries at a location corresponding to half of the total penetration distance.

3. Spray model establishment

For a diesel engine, the fuel injection is controlled by the needle valve inside the diesel fuel injector. The high-speed movement of the needle valve enables precise regulation of the diesel injection quantity. According to the classification of diesel spray breakup, it can be divided into primary breakup and secondary breakup. Primary breakup generally refers to the stage near the nozzle where the liquid jet breaks up into large-sized droplets and liquid filaments, while secondary breakup refers to the stage where the large droplets further break down into smaller droplets. Similar to diesel spray breakup, the development process of diesel spray can be mainly divided into two stages, as illustrated in Fig. 4. The first stage is characterized by the incomplete breakup of the liquid jet; the movement velocity of the liquid jet tip experiences a slight loss but remains almost consistent with the outlet velocity.

$$S_{lb(i)} = \sum_{i=1}^{n} v_{0(i)} \Delta t = k \sum_{i=1}^{n} \sqrt{\frac{2\Delta P_i}{\rho_l}} \Delta t \tag{1}$$

where $S_{lb(i)}$ denotes the moving distance of the spray tip at a certain moment in the first stage, $v_{0(i)}$ represents the nozzle outlet velocity at a specific moment, ΔP_i is the pressure inside the sac chamber at a given moment, ρ_l stands for the liquid density of diesel fuel, Δt is the time step, and k is the proportionality coefficient. The subsequent phase of spray development is characterized by a quasi-steady breakup regime. During this period, intense ambient air entrainment occurs, resulting in the formation of a consistent atomization morphology. A defining feature of this stage is that both the liquid-phase length and the spray cone angle achieve a dynamic equilibrium, exhibiting only minor temporal oscillations. The theoretical derivation and mathematical framework governing this stabilized behavior are presented in the following sections.

Fig. 5 illustrates the fuel injection rates for two injectors with different hole diameters. It can be observed that at the initial stage of injection, the injection rate increases in an almost linear manner, which implies that the outlet velocity also increases approximately linearly. As the injection rate rises to its peak value, it maintains a stable injection

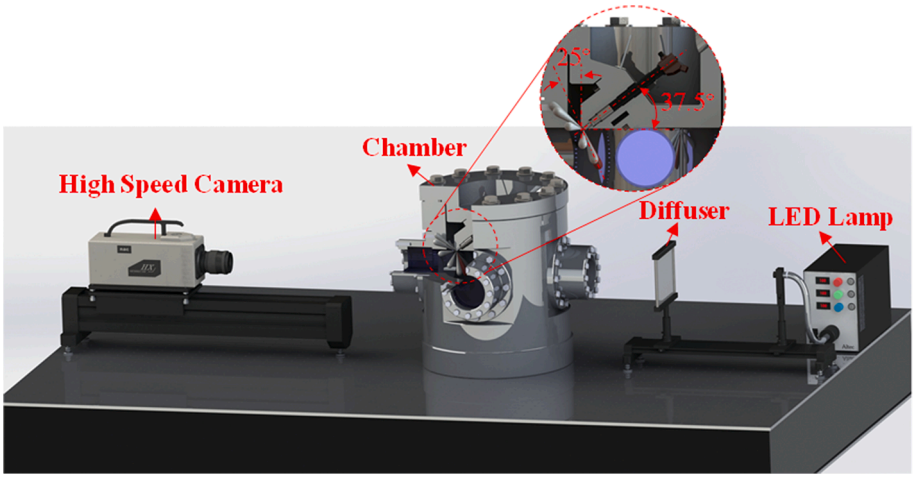


Fig. 2. Schematic representation of the DBI optical diagnostic setup and experimental configuration.

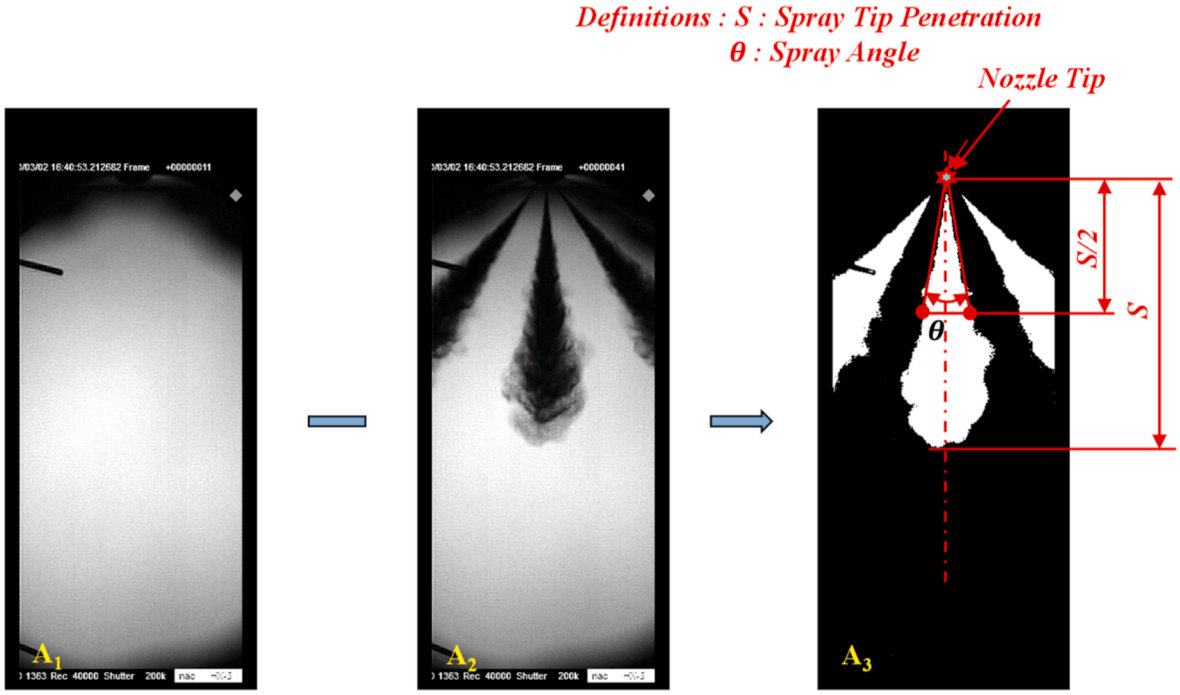
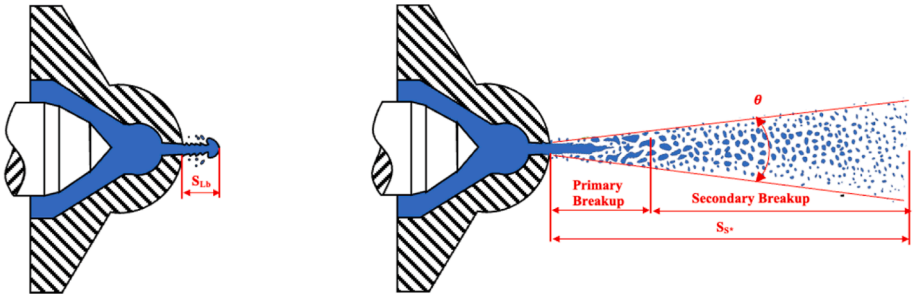
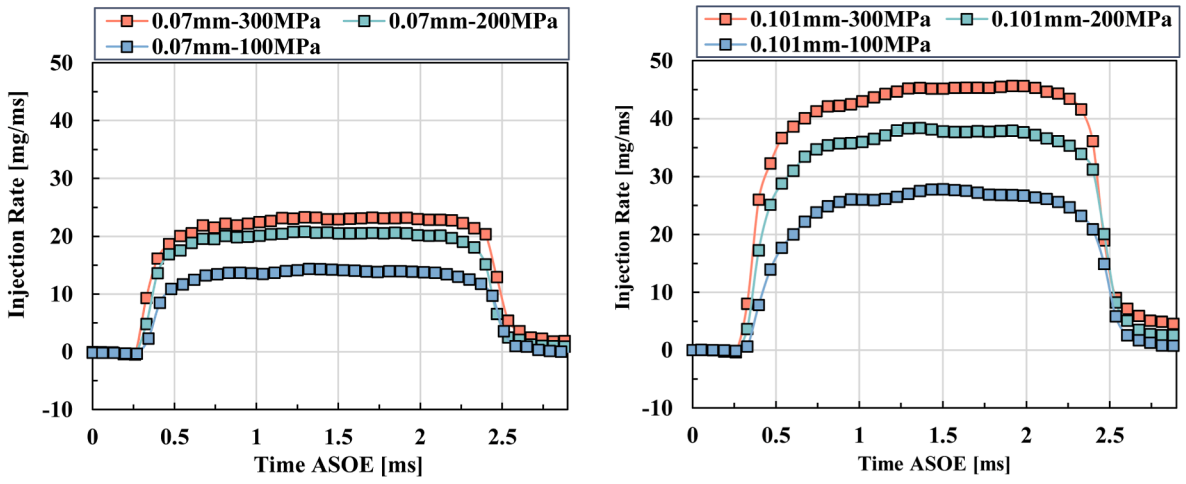


Fig. 3. Schematic of the image processing sequence and definitions of spray geometric parameters.



(a) First stage breakup (b) Second stage breakup

Fig. 4. Schematic diagram of the typical development process of fuel atomization.



(a) Injection rate of 0.07mm (b) Injection rate of 0.101mm

Fig. 5. Temporal evolution of injection rates across various operational parameters.

state. With the development of the spray, the spray enters the second stage and gradually reaches a steady state, where the spray angle and breakup length remain constant at their steady-state values.

3.1. Hypotheses

Prior to conducting the theoretical derivation of this model, the following basic assumptions are proposed:

a) The ambient gaseous medium is in a static state, and its density and thermodynamic temperature remain constant throughout the process, without fluctuations with respect to space and time.
b) The macroscopic morphology of the spray liquid jet is an axisymmetric rotating body, and all physical properties and motion parameters of the spray field satisfy the characteristic of axisymmetric distribution.
c) In the first stage of spray development, the variation in the jet velocity at the nozzle outlet directly determines and affects the advancing velocity of the spray front, and the two exhibit a linear correlation.

3.2. Theoretical model

As discussed earlier, the spray development process can be divided into two stages. In the first stage, the spray propagates in the form of a liquid jet. The duration required for the liquid jet to undergo primary atomization, known as the breakup time, was formulated by Hiroyasu et al. (Hiroyasu and Arai, 1990). This estimation is derived from fundamental hypotheses concerning the initial propagation velocity and the characteristic breakup length of the fuel jet, as expressed below:

$$Lb = 15.8D\sqrt{\frac{\rho_l}{\rho_a}} \tag{2}$$

$$tb = 28.65\frac{D\rho_l}{\sqrt{\Delta P\rho_a}} \tag{3}$$

Although the breakup length herein was obtained under steady-state conditions, it can still be used as a reference parameter considering that the time step adopted for imaging in this study is relatively large. Therefore, this paper still employs Equation (3) to distinguish between the first and second stages of spray development.

For the second stage of spray development, the liquid jet undergoes extensive breakup and forms a stable state of atomization. The motion state of the spray can be decomposed and illustrated in the steady-state spray motion analysis diagram as shown in Fig. 6. Based on the law of conservation of momentum, Equation (4) can be derived.

$$\pi\rho_l r_0^2 v_0^2 = \int_0^R 2\pi\rho_a v_{(s+1)}^2 r\mathrm{d}r \tag{4}$$

Here, ρ_l denotes the liquid fuel density, r_0 is the nozzle outlet radius, r is the radial length, v_0 represents the fuel outlet velocity, ρ_a stands for the ambient density, v_{s+1} is the velocity distribution at the (S+1)-th cross-section, and dr is the unit radial increment.

A variable δ is introduced and defined as follows in the equation:

$$\delta = \frac{r}{R_{(s+1)}} \tag{5}$$

Differentiating both sides yields:

$$\mathrm{d}\delta = \frac{\mathrm{d}r}{R_{(s+1)}} \tag{6}$$

The transverse velocity gradient within the spray plume is modeled by adopting the following functional form:

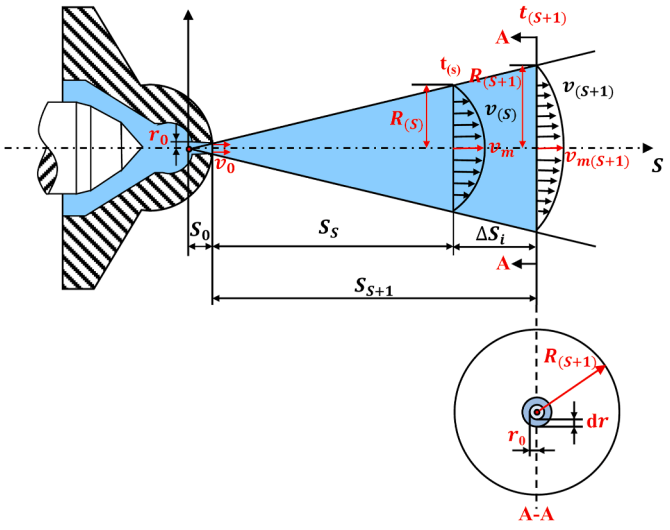


Fig. 6. Schematic illustration of the quasi-steady state during the second stage of spray development.

$$\frac{v_{(s+1)}}{v_{m(s+1)}}=\left[1-\left(\frac{r}{R_{(s+1)}}\right)^{1.5}\right]^2 \tag{7}$$

By incorporating Equation (5) into Equation (7), the following expression is obtained:

$$\left(\frac{v_{(s+1)}}{v_{m(s+1)}}\right)^2=\left[\left(1-\delta^{1.5}\right)^2\right]^2 \tag{8}$$

Simplification yields:

$$v_{(s+1)}^2=v_{m(s+1)}^2\left[\left(1-\delta^{1.5}\right)^2\right]^2 \tag{9}$$

Substituting Equation (5), Equation (6) and Equation (9) into Equation (4) yields:

$$\rho_l r_0^2 v_0^2=\int_0^R 2\pi\rho_a v_{m(s+1)}^2\left[\left(1-\delta^{1.5}\right)^2\right]^2\left(R_{(s+1)}\right)^2\delta\mathrm{d}\delta \tag{10}$$

Further simplification yields:

$$\frac{v_0}{v_{m(s+1)}}=\left(\frac{2\rho_a}{\rho_l}\right)^{0.5}\left(\frac{R_{(s+1)}}{r_0}\right)\left[\int_0^1\left[\left(1-\delta^{1.5}\right)^2\right]^2\delta\mathrm{d}\delta\right]^{0.5} \tag{11}$$

where:

$$\left[\int_0^1\left[\left(1-\delta^{1.5}\right)^2\right]^2\delta\mathrm{d}\delta\right]^{0.5}\approx 0.2154 \tag{12}$$

Simplifying Equation (11) yields:

$$v_{m(s+1)}=3.283\left(\frac{\rho_l}{\rho_a}\right)^{0.5}\frac{r_0 v_0}{R_{(s+1)}} \tag{13}$$

Based on the geometric proportional relationship illustrated in Fig. 4, it can be derived that:

$$\frac{r_0}{R_{(s+1)}}=\frac{S_0}{S_0+S_{(s+1)}}=\frac{1}{1+\frac{S_{(s+1)}\tan\left(\frac{\theta}{2}\right)}{r_0}}=\frac{r_0}{r_0+S_{(s+1)}\tan\left(\frac{\theta}{2}\right)} \tag{14}$$

Here, $S_{(s+1)}$ denotes the distance from the nozzle to the computational cross-section, θ is the spray angle, and S_0 signifies the axial offset between the nozzle orifice and the virtual origin of the spray, defined by the convergence of the projected boundary lines. By incorporating Equation (14) into Equation (13), the following relationship is derived:

$$v_{m(s+1)}=3.283\left(\frac{\rho_l}{\rho_a}\right)^{0.5}\frac{r_0 v_0}{r_0+S_{(s+1)}\tan\left(\frac{\theta}{2}\right)} \tag{15}$$

It is evident that the centerline flow velocity at a given cross-section is not numerically equivalent to the bulk propagation speed of the spray. Nevertheless, the former serves as the primary driver for the spray's axial advancement, exhibiting a clear linear correlation with the displacement rate. Consequently, a scaling factor k is incorporated to bridge these two velocities, defined as follows:

$$v_{tip(s+1)}=kv_{m(s+1)}=3.283k\left(\frac{\rho_l}{\rho_a}\right)^{0.5}\frac{r_0 v_0}{r_0+S_{(s+1)}\tan\left(\frac{\theta}{2}\right)} \tag{16}$$

In summary, the velocity expression for the spray tip penetration distance is derived. It can be observed that the spray tip velocity $v_{tip(s+1)}$ is closely correlated with the penetration distance $S_{(s+1)}$. Based on Equation (16), the velocity ratios at the same position under different operating conditions can be obtained, as shown below:

$$\frac{v'_{tip(s)}}{v''_{tip(s)}}=\frac{v'_{m(s)}}{v''_{m(s)}}=\left(\frac{\rho''_a}{\rho'_a}\right)^{0.5}\left(\frac{r'_0 v'_0}{r''_0 v''_0}\right)\left[\frac{r''_0+S_{(s)}\tan\left(\frac{\theta'}{2}\right)}{r'_0+S_{(s)}\tan\left(\frac{\theta'}{2}\right)}\right] \tag{17}$$

Where $v'_{tip(s)}$ denotes the spray tip velocity under case 1, and $v''_{tip(s)}$ represents that under case 2. If the forward displacement of the spray tip is ΔS and the spray tip velocity is assumed to remain constant over this displacement, the expression for the unit time can be obtained as shown in the following equation:

$$\Delta t=\frac{\Delta S}{v'_{tip(s)}} \tag{18}$$

The ratio of the time expressions under the two operating conditions can be expressed as:

$$\frac{\Delta t'}{\Delta t''}=\frac{v''_{tip(s)}}{v'_{tip(s)}}=\frac{v''_{m(s)}}{v'_{m(s)}}=\left(\frac{\rho'_a}{\rho''_a}\right)^{0.5}\left(\frac{r''_0 v''_0}{r'_0 v'_0}\right)\left[\frac{r'_0+S_{(s)}\tan\left(\frac{\theta'}{2}\right)}{r''_0+S_{(s)}\tan\left(\frac{\theta''}{2}\right)}\right] \tag{19}$$

Where $\Delta t'$ denotes the time required for the spray tip to travel a distance of ΔS under case 1, and $\Delta t''$ represents that under case 2. As can be observed from the above equations, for any condition, the similarity of spray penetration distances can be achieved simply by adjusting the time intervals accordingly.

$$t'_n=\sum_{i=1}^{n}\Delta t'_i=\sum_{i=1}^{n}\Delta t''_i\left(\frac{\rho'_a}{\rho''_a}\right)^{0.5}\left(\frac{r''_0 v''_0}{r'_0 v'_0}\right)\left[\frac{r'_0+S_{(i)}\tan\left(\frac{\theta'}{2}\right)}{r''_0+S_{(i)}\tan\left(\frac{\theta''}{2}\right)}\right] \tag{20}$$

A critical prerequisite for the similarity scaling of the second spray phase is the subtraction of the initial breakup duration (*tb*) characterizing the primary stage. Failure to decouple this temporal offset from the total injection time will inevitably introduce systematic deviations, undermining the fidelity of the subsequent similarity calculations.

Based on Equations (19) and (20), the spray normalization equation can thus be derived.

$$S_n=KS_n^*=K\sum_{i=1}^{n}v_{m(i)}\Delta t=K\sum_{i=1}^{n}\left(\frac{\rho_l}{\rho_a}\right)^{0.5}\frac{r_0 v_0}{r_0+S_{(i)}\tan\left(\frac{\theta}{2}\right)}\Delta t \tag{21}$$

Based on the authors' previous research, the spray angle is generally correlated with four parameters, namely the pressure difference ΔP, fuel density ρ_l, air density ρ_a, and nozzle diameter D, and satisfies the following equation:

$$\tan\left(\frac{\theta}{2}\right)\propto\left(\frac{\rho_a}{\rho_l}\right)^{b1}(D)^{b2}(\Delta P)^{b3} \tag{22}$$

For single-fuel applications, the similarity equation for the spray angle can be derived as follows:

$$\frac{\tan\left(\frac{\theta_1}{2}\right)}{\tan\left(\frac{\theta_2}{2}\right)}=\left(\frac{\rho_{a1}}{\rho_{a2}}\right)^{b1}\left(\frac{D_1}{D_2}\right)^{b2}\left(\frac{\Delta P_1}{\Delta P_2}\right)^{b3} \tag{23}$$

Based on Equations (22) and (23), the normalization equation for the spray angle can thus be derived:

$$\beta_\theta=\frac{\tan\left(\frac{\theta}{2}\right)}{\left(\frac{\rho_a}{\rho_l}\right)^{b1}(D)^{b2}(\Delta P)^{b3}} \tag{24}$$

4. Experimental results and discussion

Fig. 7 illustrates the spray tip penetration calculated from the spray images acquired via the DBI method illustrated in Fig. 2, with the image processing methodology detailed in Fig. 3. Quantitative results for spray tip penetration are partitioned by nozzle diameter: 0.07 mm in subfigure (a) and 0.101 mm in subfigure (b). These visualizations capture the dynamic response of the fuel plume to varying rail pressures and ambient densities. Notably, the surrounding gas density emerges as the most sensitive parameter, exerting a profound impact on the penetration rate that overshadows the effects of injection pressure variations. Although the injection pressure also alters the penetration, its effect is relatively weak in comparison with that of the ambient density. In addition, the hole diameter contributes to the variation in penetration as well, and the specific variation characteristics have been discussed in previous studies, which will not be elaborated further herein (Zhai et al., 2021, 2023).

Fig. 8 delineates the processed spray angles for two distinct injector geometries. The small hole injector of 0.07 mm is represented in subfigure (a), while the results for the larger hole injector of 0.101 mm are detailed in subfigure (b). This data set enables a direct comparison of the near-field atomization behavior as a function of the nozzle exit diameter. Both subfigures incorporate the results under different injection pressures and ambient densities. It can be observed from the figures that the injection pressure exerts a relatively minor effect on the spray angle, while the ambient density and hole diameter are the key influencing factors. Specifically, an increase in the ambient density and hole diameter directly promotes the enlargement of the spray angle.

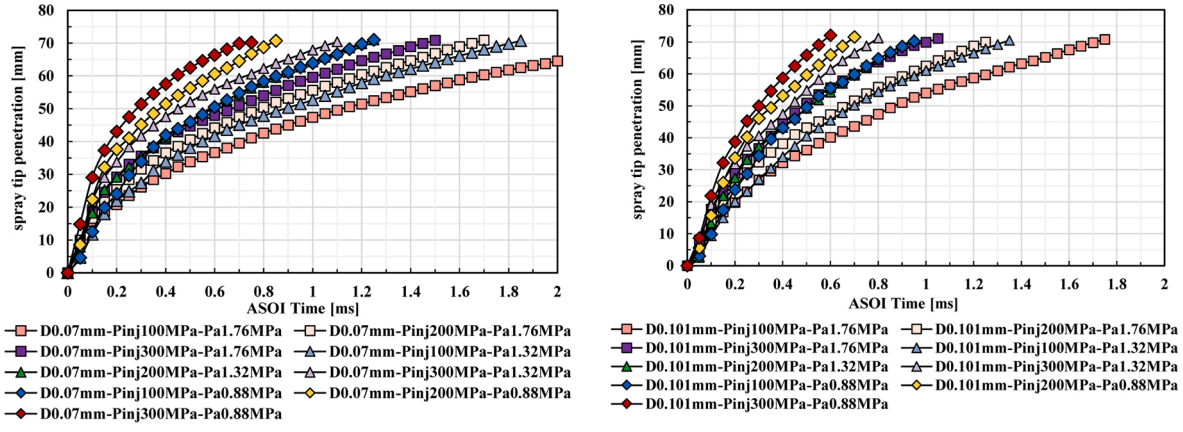
In light of the preceding analysis, it is evident that the ambient gas density, injection pressure, and nozzle orifice diameter collectively dictate the macro-morphological evolution of the spray. These parameters serve as the primary drivers, modulating the momentum exchange and spatial distribution of the fuel plume throughout the injection event. Therefore, the key lies in how to consider these various factors to achieve the similarity and normalization of spray characteristics. Through the previous analysis, the spray has been divided into two main stages. According to Equation (21), a normalized structural analysis was performed on the spray data of the second stage, and the results are illustrated in Fig. 9. Herein, the ordinate represents the actual spray tip penetration (S), while the abscissa denotes the theoretical spray tip penetration S* calculated by Equation (21). The scattered points in the figure correspond to the actual experimental data. It can be clearly observed from the figure that under all operating conditions, there exists an obvious linear correlation between the actual spray tip penetration S and the theoretical spray tip penetration S*, and effective normalization can be realized across different operating conditions. Furthermore, this indicates that through the normalized mathematical equation, the variation of spray tip penetration with time at any moment can be calculated, which can be applied to the development of a mathematical model for spray tip penetration. Therefore, a linear fitting was conducted on the linear relationship between the actual spray tip penetration S and the theoretical penetration S*. The fitting result is presented as the red solid line in Fig. 9, and the corresponding mathematical expression is obtained as follows:

$$S = 0.4287 S_n^* + 8.684 \tag{25}$$

The final fitting result yields a coefficient of determination $R^2 = 0.9767$, which indicates a distinct linear correlation between the two variables. Furthermore, Fig. 9 reveals a noticeable dispersal in the spray tip penetration data during the initial phase, particularly within the highlighted red zone where penetration distances remain limited. However, as the spray progresses downstream, these fluctuations diminish, and the penetration profiles converge toward a distinct linear progression. This indirectly verifies that the initial movement of the spray does not conform to the second stage trend of the spray, which is consistent with the conclusion proposed in this study that the spray movement can be divided into two stages. Although the data within the breakup time have been partially excluded in Fig. 9 with Equation (3) as the demarcation point, this phenomenon still exists. This implies that the existing prediction equation for spray breakup time is not sufficiently accurate, and the duration of this stage is underestimated. Therefore, it is necessary to conduct more detailed research on the duration and length of the first stage of spray development.

Based on Equation (20), similarity conversion was performed on the spray tip penetration under different conditions, and the converted results are illustrated in Fig. 10. The 0.07 mm diameter injector, operating under a 100 MPa injection pressure and an ambient density of 10 kg/m^3, was selected as the reference case for the similarity normalization process. In Fig. 10, the red solid line with white hollow markers represents the baseline conditions, while the scattered points of other colors denote the converted results under other operating conditions. It can be observed from the figure that the conversion of spray tip penetration under different operating conditions was successfully achieved via Equation (20), with the converted results exhibiting good consistency.

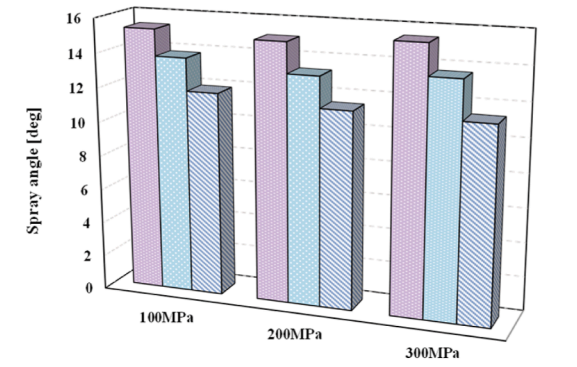
To further clarify the practical applicability of the proposed model, it should be emphasized that the present formulation provides a direct and implementable approach for predicting spray penetration under engineering conditions. Specifically, by combining Eq. (21) with Eq. (25), the



(a) Analysis results of spray tip penetration for the hole diameter of 0.07 mm

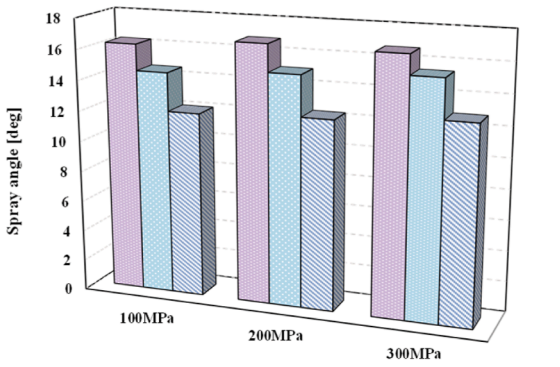
(b) Analysis results of spray tip penetration for the hole diameter of 0.101 mm

Fig. 7. Parametric analysis of spray tip penetration across diverse boundary conditions.



	100MPa	200MPa	300MPa
20kg/m3	15.33912113	15.06304262	15.45818756
15kg/m3	13.79516162	13.2852583	13.6560937
10kg/m3	11.90085623	11.48574376	11.38574376

(a) Analysis results of spray angle for the hole diameter of 0.07 mm



	100MPa	200MPa	300MPa
20kg/m3	16.3	16.83091	16.738123
15kg/m3	14.593386	15.045915	15.445915
10kg/m3	12.094479	12.394479	12.894479

(b) Analysis results of spray angle for the hole diameter of 0.101 mm

Fig. 8. Parametric analysis of the spray angle characteristics across diverse boundary conditions.

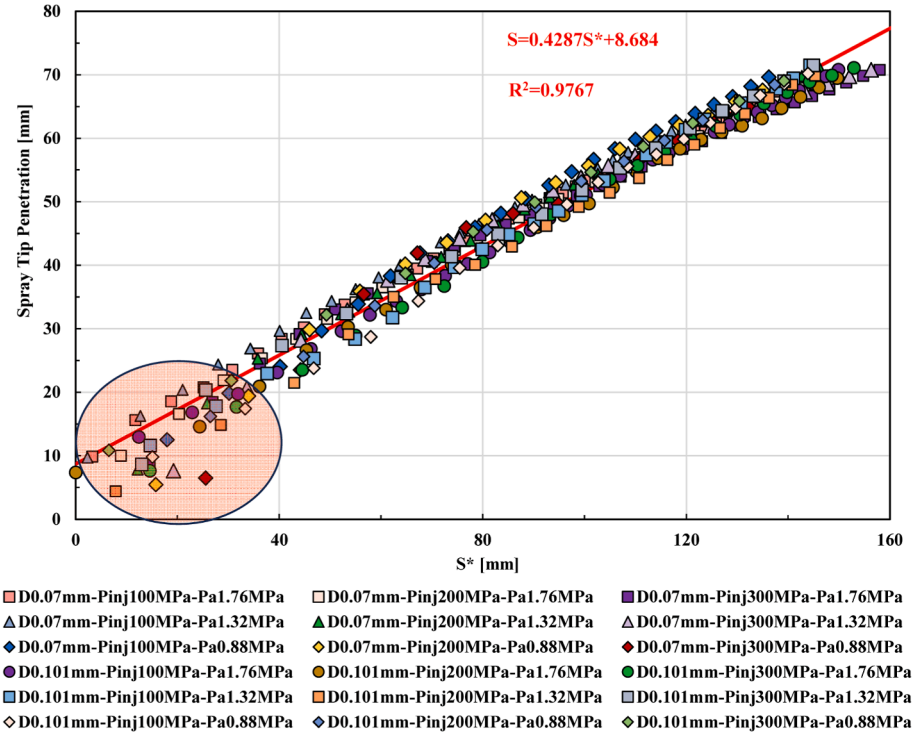
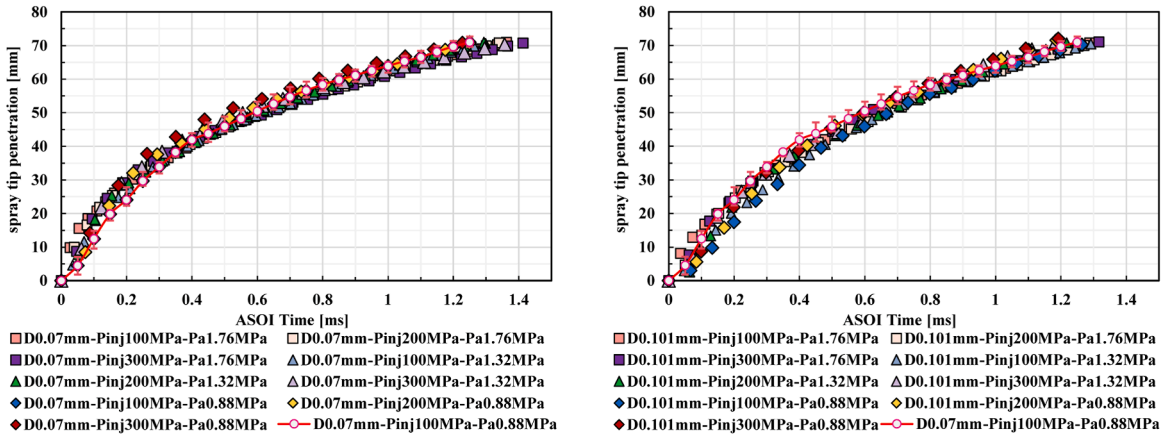


Fig. 9. Normalization result of spray tip penetration across diverse boundary conditions.

spray penetration can be readily determined once the operating parameters (e.g., injection pressure, nozzle diameter, and ambient density) are specified. The normalization framework enables the transformation of different injection conditions into a unified similarity space, and the penetration evolution can then be obtained through the derived scaling relationships. This approach allows for rapid estimation of spray development without the need for extensive experimental calibration, and is therefore particularly useful in the preliminary design and optimization of fuel injection systems. In addition, the model can be applied to scale spray behavior across different operating conditions, significantly reducing the experimental effort required for performance evaluation.

Based on Equation (22), we have demonstrated that the tangent value of the spray angle is correlated with environmental density, fuel density, hole diameter, and differential injection pressure. Therefore, based on Equation (23), all the spray angle data were subjected to fitting analysis, and the parameters b1, b2, and b3 were derived. From the fitting results, the following equation is obtained:



(a) Similarization results of spray tip penetration for the hole diameter of 0.07 mm

(b) Similarization results of spray tip penetration for the hole diameter of 0.101 mm

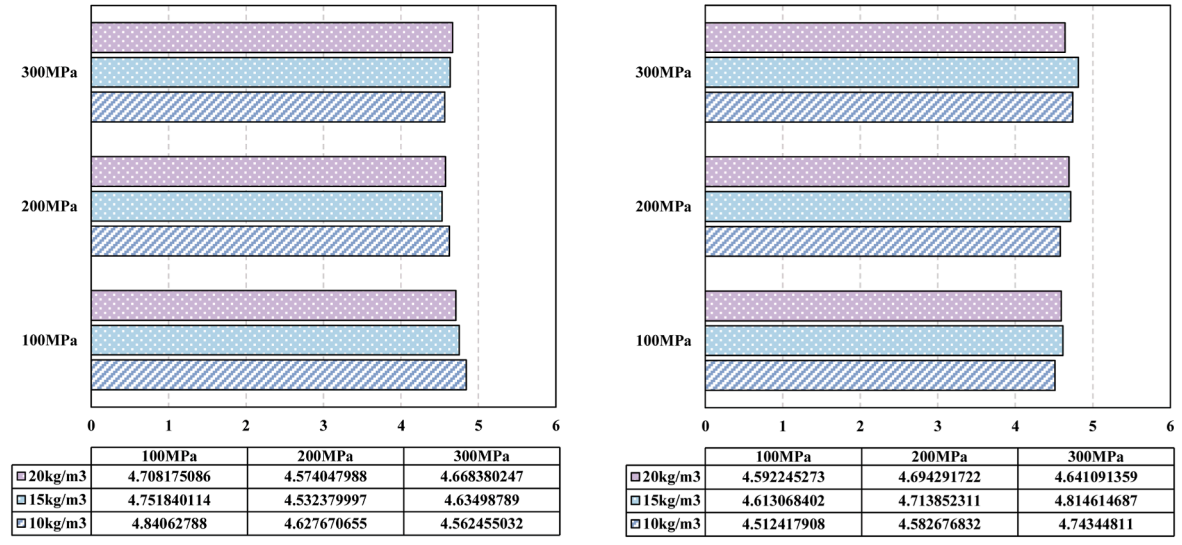
Fig. 10. Similarization results of penetration across diverse boundary conditions.

$$\frac{\tan\left(\frac{\theta_1}{2}\right)}{\tan\left(\frac{\theta_2}{2}\right)} = \left(\frac{\rho_{a1}}{\rho_{a2}}\right)^{0.41316}\left(\frac{D_1}{D_2}\right)^{0.23585}\left(\frac{\Delta P_1}{\Delta P_2}\right)^{0.013245} \tag{26}$$

Herein, $b1 = 0.41316$, $b2 = 0.23585$ and $b3 = 0.013245$. The coefficient of determination of the fitting result is $R^2 = 0.976$, which indicates that the fitting result is satisfactory. Using these results, a normalization analysis was conducted on the experimental data, and the results are presented in Fig. 11. Specifically, subfigure (a) shows the normalized results of the spray angle for the injector with a nozzle orifice diameter of 0.07 mm, while subfigure (b) illustrates those for the injector with a nozzle orifice diameter of 0.101 mm. It can be observed from the figures that the normalization results of the spray angle are favorable, with the normalized spray angle being approximately 4.6. The specific value of 4.656 can be obtained by averaging all the data values. Substituting this value into Equation (22) yields the prediction equation for the spray angle as follows:

$$\tan\left(\frac{\theta}{2}\right) = 4.656\left(\frac{\rho_a}{\rho_l}\right)^{0.41316}(D)^{0.23585}(\Delta P)^{0.013245} \tag{27}$$

Based on Equation (26), a similarity analysis was conducted on the spray angle, where the similarity normalization was referenced to the injector with a hole diameter of 0.07 mm, at an ambient density of 20 kg/m^3 and an injection pressure of 100 MPa. The baseline conditions were scaled according to Equation (26), and the results are illustrated in Fig. 12. Specifically, subfigure (a) corresponds to the conditions of the injector with a nozzle orifice diameter of 0.07 mm, while subfigure (b) corresponds to those of the injector with a nozzle orifice diameter of



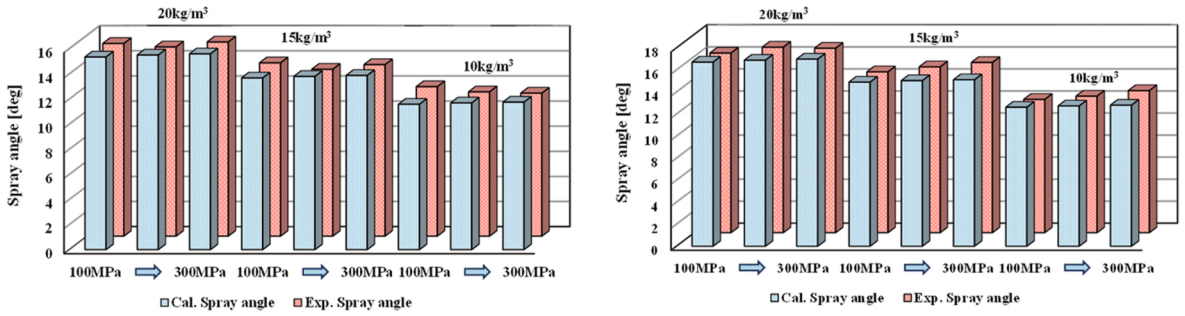
	100MPa	200MPa	300MPa
20kg/m3	4.708175086	4.574047988	4.668380247
15kg/m3	4.751840114	4.532379997	4.63498789
10kg/m3	4.84062788	4.627670655	4.562455032

	100MPa	200MPa	300MPa
20kg/m3	4.592245273	4.694291722	4.641091359
15kg/m3	4.613068402	4.713852311	4.814614687
10kg/m3	4.512417908	4.582676832	4.74344811

(a) Normalization result of spray angle for the hole diameter of 0.07 mm

(b) Normalization result of spray angle for the hole diameter of 0.101 mm

Fig. 11. Normalization result of spray angle across diverse boundary conditions.



(a) Similarization result of spray angle for the hole diameter of 0.07 mm

(b) Similarization result of spray angle for the hole diameter of 0.101 mm

Fig. 12. Similarization result of spray angle across diverse boundary conditions.

0.101 mm. In the figures, the blue histograms represent the scaled results calculated via Equation (26), and the red histograms denote the experimental results. It can be observed that the spray angle can be satisfactorily predicted using the similarity principle, which also indicates that the spray angles under different conditions can be converted via the similarity method.

5. Conclusions

Aiming at the lack of research on mathematical models for the similarity and normalization of diesel engine spray characteristics under ultra-high pressure and micro-hole conditions, this paper conducts systematic theoretical derivation and experimental verification research focusing on two core spray characteristics: spray tip penetration and spray angle. The main conclusions are as follows:

By dividing the spray development process into two stages and selecting injection pressure difference, ambient density, and nozzle hole diameter as the key influencing variables, this study derived and established the similarity criteria and normalization equations for spray tip penetration and spray angle. Combined with the DBI method and image processing technology, experimental data were obtained; taking the nozzle with an orifice diameter of 0.07 mm, an injection pressure of 100 MPa, and an ambient density of 10 kg/m^3 as the base condition, the similarity conversion verification of spray characteristics under different operating conditions was completed. In addition, dimensionless verification was carried out on the spray tip penetration under various conditions, with the correlation coefficient R^2 of the verification results reaching 0.9767. Meanwhile, research on the similarity and normalization of spray angles was conducted, and the results showed good consistency with the experimental data, which verified the reliability and accuracy of the established models. Moreover, this study found that the initial movement of the spray does not conform to the expansion trend, revealing that the existing prediction equation for spray breakup time has an underestimation bias, which provides a direction for the subsequent refined research on the first stage of spray development.

In conclusion, the similarity criteria and normalization equations for spray characteristics established in this paper can provide important theoretical support for the spray characteristic prediction of ultra-high pressure small high-speed diesel engines and also lay a foundation for the design and performance regulation of ultra-high pressure small high-speed internal combustion engine power systems. Future research can be further extended to the spray characteristic analysis of alternative fuels and the construction of spray-combustion coupling models, so as to improve the theoretical system of internal combustion engine power systems.

CRediT authorship contribution statement

Meiqi Yu: Writing – original draft. **Hongliang Luo:** Supervision, Funding acquisition. **Weidi Huang:** Supervision, Funding acquisition. **Pengbo Dong:** Supervision, Data curation. **Yu Jin:** Software, Data curation. **Keiya Nishida:** Supervision, Project administration, Funding acquisition. **Chang Zhai:** Writing – review & editing, Writing – original draft, Data curation. **Xiaoqing Tian:** Software, Data curation.

Declaration of competing interest

The authors declare that they have no known competing financial interests or personal relationships that could have appeared to influence the work reported in this paper.

Acknowledgements

This research was supported by the Fundamental Research Funds for the Central Universities (grant numbers 3072025CFJ0703, 30720205GH0301, 3072025PT0302, and 3072025CFJ0303). The authors would like to thank Mazda for supplying the injection system and Nac for offering technical support.

References

An, C., Liu, L., Luo, H., Xiong, Q., Zhou, B., Liu, Y., Li, X., Nishida, K., 2025. Experimental and modeling study of the ultra-high pressure spray dynamics in the near and far fields under high ambient density conditions. Energy, 138464. https://doi.org/10.1016/j.energy.2025.138464.

Arai, M., 2022. Interpretative review of diesel spray penetration normalized by length and time of breakup (similarity law of diesel spray and its application). Energies 15 (13), 4926. https://doi.org/10.3390/en15134926.

Arrègle, J., Pastor, J.V., Ruiz, S., 1999. The influence of injection parameters on diesel spray characteristics (No. 1999-01-0200). https://doi.org/10.4271/1999-01-0200.

Bergin, M., Reitz, R.D., Hessel, R.P., 2005. Soot and NOx emissions reduction in diesel engines via spin-spray combustion. In: ILASS American, 18th Annual Conference on Liquid Atomization Spray Systems, Irvine, CA.

Chen, P.C., Wang, W.C., Roberts, W.L., Fang, T., 2013. Spray and atomization of diesel fuel and its alternatives from a single-hole injector using a common rail fuel injection system. Fuel 103, 850–861. https://doi.org/10.1016/j.fuel.2012.08.013.

Dent, J.C., 1971. A basis for the comparison of various experimental methods for studying spray penetration. SAE Trans. 1881–1884. https://www.jstor.org/stable/44651829.

Delacourt, E., Desmet, B., Besson, B., 2005. Characterisation of very high pressure diesel sprays using digital imaging techniques. Fuel 84 (7–8), 859–867. https://doi.org/10.1016/j.fuel.2004.12.003.

Desantes, J.M., Payri, R., Salvador, F.J., Gil, A., 2006a. Development and validation of a theoretical model for diesel spray penetration. Fuel 85 (7–8), 910–917. https://doi.org/10.1016/j.fuel.2005.10.023.

Desantes, J.M., Payri, R., Salvador, F.J., Gimeno, J., 2006b. Prediction of spray penetration by means of spray momentum flux. SAE Technical Paper Series. https://doi.org/10.4271/2006-01-1387.
Gerald Liu, Z., Munnannur, A., 2019. Future diesel engines. In: Design and Development of Heavy Duty Diesel Engines. a Handbook. Springer Singapore, Singapore, pp. 887–914. https://doi.org/10.1007/978-981-15-0970-4_24.
Hiroyasu, H., Arai, M., 1990. Structures of fuel sprays in diesel engines. SAE Trans. 1050–1061. https://www.jstor.org/stable/44548562.
Inagaki, K., Mizuta, J., Kawamura, K., Idota, Y., Hashizume, T., 2016. Theoretical study on spray design for small-bore diesel engine (No. 2016-01-0740). SAE Technical Paper. https://doi.org/10.4271/2016-01-0740.
Jia, T.M., Li, G.X., Yu, Y.S., Xu, Y.J., 2016a. Effects of ultra-high injection pressure on penetration characteristics of diesel spray and a two-mode leading edge shock wave. Exp. Therm. Fluid Sci. 79, 126–133. https://doi.org/10.1016/j.expthermflusci.2016.07.006.
Jia, T.M., Li, G.X., Yu, Y.S., Xu, Y.J., 2016b. Propagation characteristics of induced shock waves generated by diesel spray under ultra-high injection pressure. Fuel 180, 521–528. https://doi.org/10.1016/j.fuel.2016.04.009.
Jin, Y., Zhai, C., Nishida, K., Ogata, Y., 2020. An analysis of diesel spray characteristics with small injection amount under similarity law condition. Small Engine Technol. Conf. Expo. 308417. https://doi.org/10.4271/2019-32-0590.
Kostas, J., Honnery, D., Soria, J., 2009. Time resolved measurements of the initial stages of fuel spray penetration. Fuel 88 (11), 2225–2237. https://doi.org/10.1016/j.fuel.2009.05.013.
Kothiwale, G.R., Akkoli, K.M., Doddamani, B.M., Kattimani, S.S., Ağbulut, Ü., Afzal, A., Kaladgi, A.R., Said, Z., 2023. Impact of injector nozzle diameter and hole number on performance and emission characteristics of CI engine powered by nanoparticles. Int. J. Environ. Sci. Technol. 20, 5013–5034. https://doi.org/10.1007/s13762-022-04397-0, 2023.
Luo, H., Jin, Y., Zhai, C., Chang, F., Xing, W., Nishida, K., Ogata, Y., 2023. Very low soot formation with modulated liquid length and lift-off length of diesel spray flame. J. Energy Inst. 111, 101383. https://doi.org/10.1016/j.joei.2023.101383.
Mohan, B., Yang, W., kiang Chou, S., 2013. Fuel injection strategies for performance improvement and emissions reduction in compression ignition engines—A review. Renew. Sustain. Energy Rev. 28, 664–676. https://doi.org/10.1016/j.rser.2013.08.051.
Murugesan, A., Umarani, C., Subramanian, R., Nedunchezhian, N., 2009. Bio-diesel as an alternative fuel for diesel engines—a review. Renew. Sustain. Energy Rev. 13 (3), 653–662. https://doi.org/10.1016/j.rser.2007.10.007.
Ouyang, G., An, S., Liu, Z., Li, Y., 2019. Common Rail Fuel Injection Technology in Diesel Engines. John Wiley & Sons.
Pandey, R.K., Rehman, A., Sarviya, R.M., 2012. Impact of alternative fuel properties on fuel spray behavior and atomization. Renew. Sustain. Energy Rev. 16 (3), 1762–1778. https://doi.org/10.1016/j.rser.2011.11.010.
Park, S.H., Youn, I.M., Lim, Y., Lee, C.S., 2013. Influence of the mixture of gasoline and diesel fuels on droplet atomization, combustion, and exhaust emission characteristics in a compression ignition engine. Fuel Process. Technol. 106, 392–401. https://doi.org/10.1016/j.fuproc.2012.09.004.
Siebers, D.L., 1998. Liquid-phase fuel penetration in diesel sprays. SAE Trans. 1205–1227. https://www.jstor.org/stable/44736606.
Stager, L.A., Reitz, R.D., 2007. Assessment of diesel engine size-scaling relationships (No. 2007-01-0127). SAE Technical Paper. https://doi.org/10.4271/2007-01-0127.
Shi, Y., Reitz, R.D., 2008. Study of diesel engine size-scaling relationships based on turbulence and chemistry scales (No. 2008-01-0955). SAE Technical Paper. https://doi.org/10.4271/2008-01-0955.
Suzuki, T., Ohshima, R., 2002. An experimental Study on diesel spray Behavior—Non-dimensional expression for spray Tip penetration. Mar. Eng. 37 (3), 213–219. https://doi.org/10.5988/jime.37.213.
Vera-Tudela, W., Haefeli, R., Barro, C., Schneider, B., Boulouchos, K., 2020. An experimental study of a very high-pressure diesel injector (up to 5000 bar) by means of optical diagnostics. Fuel 275, 117933. https://doi.org/10.1016/j.fuel.2020.117933.
Wang, L., Lowrie, J., Ngaile, G., Fang, T., 2019. High injection pressure diesel sprays from a piezoelectric fuel injector. Appl. Therm. Eng. 152, 807–824. https://doi.org/10.1016/j.applthermaleng.2019.02.095.
Wakuri, Y., Fujii, M., Amitani, T., Tsuneya, R., 1960. Studies on the penetration of fuel spray in a diesel engine. Bull.JSME 3 (9), 123–130. https://doi.org/10.1299/jsme1958.3.123.
Xin, Q., 2011. Diesel Engine System Design. Elsevier.
Xia, J., Huang, Z., Xu, L., Ju, D., Lu, X., 2019. Experimental study on spray and atomization characteristics under subcritical, transcritical and supercritical conditions of marine diesel engine. Energy Convers. Manag. 195, 958–971. https://doi.org/10.1016/j.enconman.2019.05.080.
Yu, S., Yu, M., Sun, P., Wang, J., Xu, J., 2026. Spray and combustion characteristics of−10 diesel and− 50 biodiesel under various injection pressures in a constant-volume combustion chamber. Energy 342, 139688. https://doi.org/10.1016/j.energy.2025.139688.
Zhai, C., Jin, Y., Nishida, K., Ogata, Y., 2021a. Diesel spray and combustion of multi-hole injectors with micro-hole under ultra-high injection pressure–non-evaporating spray characteristics. Fuel 283, 119322. https://doi.org/10.1016/j.fuel.2020.119322.
Zhai, C., Jin, Y., Wu, Q., Nishida, K., Ogata, Y., 2021b. Diesel spray and combustion of multi-hole injectors with micro-hole under ultra-high injection pressure–combustion characteristics. Fuel 300, 120949. https://doi.org/10.1016/j.fuel.2021.120949.
Zhai, C., Zhang, G., Jin, Y., Nishida, K., Ogata, Y., Luo, H., 2022a. Characterization of diesel spray combustion using two-color pyrometry and OH* chemiluminescence imaging-comparison between micro-hole and ultra-high injection pressure effects. J. Energy Inst. 103, 104–116. https://doi.org/10.1016/j.joei.2022.05.012.
Zhai, C., Jin, Y., Wu, Q., Nishida, K., Ogata, Y., 2022b. Diesel spray of multi-hole injectors with micro-hole under ultra-high injection pressure-evaporating spray characteristics. Atomization Sprays 32 (1). https://doi.org/10.1615/AtomizSpr.2021037966.
Zhai, C., Chang, F., Jin, Y., Luo, H., 2023a. Investigations on the diesel spray characteristic and tip penetration model of multi-hole injector with micro-hole under ultra-high injection pressure. Sustainability 15 (14), 11114. https://doi.org/10.3390/su151411114.
Zhai, C., Jin, Y., Feng, Z., Chang, F., Luo, H., Nishida, K., Ogata, Y., 2023b. Characterization of diesel spray combustion under micro-hole and ultra-high injection pressure conditions-analyses of diffused back-illumination imaging and OH* chemiluminescence imaging. Fuel Process. Technol. 252, 107955. https://doi.org/10.1016/j.fuproc.2023.107955.
Zhai, C., Liu, E., Zhang, G., Xing, W., Chang, F., Jin, Y., Luo, H., Nishida, K., Ogata, Y., 2024. Similarity and normalization study of fuel spray and combustion under ultra-high injection pressure and micro-hole diameter conditions–spray characteristics. Energy 288, 129684. https://doi.org/10.1016/j.energy.2023.129684.
Zhai, C., Zhang, J., Li, K., Dong, P., Jin, Y., Chang, F., Luo, H., 2025. Comparative analysis and normalization of single-hole vs. multi-hole spray characteristics: 1st report on spray characteristic comparison. Green Energy Resour. 3 (1), 100120. https://doi.org/10.1016/j.gerr.2025.100120.
Zhou, X., Li, T., Lai, Z., Wang, B., 2018. Scaling fuel sprays for different size diesel engines. Fuel 225, 358–369. https://doi.org/10.1016/j.fuel.2018.03.167.
Zhou, X., Li, T., 2021. Modeling of the entire processes of diesel spray tip penetration including the start-and end-of-injection transients. J. Energy Inst. 98, 271–281. https://doi.org/10.1016/j.joei.2021.07.007.
Zhou, Y., Pei, J., Ding, S., Zhao, S., Zhu, K., Shao, L., Zhong, Z., Du, F., Li, X., Xu, Z., 2024. Theoretical model for high-altitude gas exchange process in multi-fuel poppet valves two-stroke aircraft engine. Energy Convers. Manag. 301, 118028. https://doi.org/10.1016/j.enconman.2023.118028.
Zhang, J., Feng, Z., Gu, J., Jin, Y., Leng, X., Huang, R., He, Z., 2026. Decoupling the effect of viscosity and surface tension on fuel atomization characteristics. Phys. Fluids 38 (1). https://doi.org/10.1063/5.0309846.